Temperature-Induced Lifshitz Transition in WTe_2

Yun Wu,[1] Na Hyun Jo,[1] Masayuki Ochi,[2,3] Lunan Huang,[1] Daixiang Mou,[1] Sergey L. Bud'ko,[1] P. C. Canfield,[1,*] Nandini Trivedi,[4] Ryotaro Arita,[2,3] and Adam Kaminski[1,†]

[1]*Ames Laboratory, U.S. DOE and Department of Physics and Astronomy, Iowa State University, Ames, Iowa 50011, USA*

[2]*RIKEN Center for Emergent Matter Science (CEMS), Wako, Saitama 351-0198, Japan*

[3]*JST ERATO Isobe Degenerate π-Integration Project, Advanced Institute for Materials Research (AIMR), Tohoku University, Sendai, Miyagi 980-8577, Japan*

[4]*Department of Physics, The Ohio State University, Columbus, Ohio 43210, USA*

(Received 10 June 2015; revised manuscript received 6 August 2015; published 12 October 2015)

We use ultrahigh resolution, tunable, vacuum ultraviolet laser-based, angle-resolved photoemission spectroscopy (ARPES), temperature- and field-dependent resistivity, and thermoelectric power (TEP) measurements to study the electronic properties of WTe_2, a compound that manifests exceptionally large, temperature-dependent magnetoresistance. The Fermi surface consists of two pairs of electron and two pairs of hole pockets along the X-Γ-X direction. Using detailed ARPES temperature scans, we find a rare example of a temperature-induced Lifshitz transition at $T \simeq 160$ K, associated with the complete disappearance of the hole pockets. Our electronic structure calculations show a clear and substantial shift of the chemical potential $\mu(T)$ due to the semimetal nature of this material driven by modest changes in temperature. This change of Fermi surface topology is also corroborated by the temperature dependence of the TEP that shows a change of slope at $T \approx 175$ K and a breakdown of Kohler's rule in the 70–140 K range. Our results and the mechanisms driving the Lifshitz transition and transport anomalies are relevant to other systems, such as pnictides, 3D Dirac semimetals, and Weyl semimetals.

DOI: 10.1103/PhysRevLett.115.166602 PACS numbers: 72.15.Gd, 71.15.Mb, 71.20.Be, 79.60.Bm

Traditional phase transitions are driven by spontaneous symmetry breaking and the continuous growth of an order parameter below the transition, as in magnets and superconductors. In addition, it is possible to have phase transitions in topological materials that do not break any symmetries but can be described by topological invariants. Here we describe a fundamentally different type of phase transition in fermionic systems, a Lifshitz transition, that involves a change of the Fermi surface topology. Such Lifshitz transitions hold the key to new types of topological phase transitions [1,2]. Lifshitz transitions driven by chemical doping or substitution [3,4] or pressure [5,6] are common and have been observed previously. In this Letter, we provide evidence for a new type of such transition that is driven by temperature.

From the giant magnetoresistance (MR) in Fe/Cr superlattice [7,8], to colossal MR in manganese oxide materials [9–11], these phenomena have opened a new era of applications in magnetic field sensors, read heads in high density hard disks, random access memories, and galvanic isolators [12]. Recently, extremely large MR has been observed in $PtSn_4$ [13], Cd_3As_2 [14], $NbSb_2$ [15], and WTe_2 [16]. In both $PtSn_4$ and WTe_2, the MR shows no sign of saturation and reaches an order of at least 10^5% at low temperature. The MR in WTe_2 also displays large 3D anisotropy [17,18] and is linear up to 60 T [17,19]. Different mechanisms have been proposed to explain MR in these materials [13,14,16,20,21]. However, the exact origin of MR in these materials remains an open question.

WTe_2 has been known for several decades now [22], and a phenomenological three-carrier semimetal band model [22,23], density-functional-based augmented spherical wave electronic structure calculations, and early, relatively low resolution angle-resolved photoemission spectroscopy (ARPES) [24] have supported the semimetallic nature of this material. Recent quantum oscillation [25–27] results have revealed the presence of four small electron and four small hole pockets of roughly similar size consistent with ARPES data [20]. These findings are consistent with carrier compensation mechanisms as the primary source of the MR effect [16,21]. Furthermore, ARPES studies [20] also reported a change of the size of the Fermi pockets between 20 and 100 K. More recently, Jiang *et al.* [28] have proposed that protection from backscattering could play a role in the large nonsaturating MR of WTe_2 in the presence of strong spin-orbital coupling effects. Amazingly, Kang *et al.* demonstrated that a suppression of the magnetoresistence with pressure in this material leads to emergence of superconductivity with respectable T_c of ~6.5 K [6]. This occurs in the absence of structural transition, and is caused by pressure-induced Lifshitz transition (suppression of hole pockets), as is evident from Hall data [6].

The strength of our Letter is the combination of temperature-dependent ultrahigh resolution, tunable vacuum ultraviolet (VUV) laser based ARPES [29], and

temperature- and field-dependent resistivity and thermoelectric power (TEP) measurements, that together with electronic structure calculations provide new insights into the mechanisms driving the phenomena we observe. The electronic structure calculations show, and our data are consistent with, the presence of two pairs of hole pockets and two pairs of nearly degenerate electron pockets along the X-Γ-X direction. Systematic temperature-dependence measurements reveal for the first time a Lifshitz transition, i.e., a change of the Fermi surface topology, close to 160 K, above which both pairs of hole pockets vanish. We further show that this transition is associated with a change of slope observed in the derivative of the temperature-dependent TEP. We demonstrate that the shift of the chemical potential (μ) with temperature, responsible for the Lifshitz transition, is caused by the close proximity of electron and hole densities of states near the Fermi energy. This result is applicable to other important semimetallic systems, such as pnictides, 3D Dirac semimetals, and Weyl semimetals.

Whereas most of the previous measurements have been carried out on WTe_2 crystals grown via chemical vapor transport using halogens as transport agents [16,30], we have grown WTe_2 single crystals from a Te-rich binary melt. High-purity, elemental W and Te were placed in alumina crucibles in W_1Te_{99} and W_2Te_{98} ratios. The crucibles were sealed in amorphous silica tubes and the ampoules were heated to 1000 °C over 5 h, held at 1000 °C for 10 h, then slowly cooled to 460 °C over 100 h, and finally decanted using a centrifuge [31]. The resulting crystals were blade- or ribbonlike in morphology with typical dimensions of $3 \times 0.5 \times 0.01$ mm with the crystallographic c axis being perpendicular to the larger crystal surface; the crystals are readily cleaved along this crystal surface. Temperature- and field-dependent transport measurements were performed in a Quantum Design Physical Property Measurement System for $1.8 \leq T \leq 350$ K and $|H| \leq 140$ kOe. The TEP measurements were performed by a dc alternating temperature gradient technique [32]. Temperature- and field-dependent resistivity measurements made on our solution grown samples (see Figs. S1–S3 of the Supplemental Material [33]) demonstrate exceedingly high values of the residual resistivity ratio in excess of 900 and MR values at 1.8 K and 90 kOe up to 6×10^5%. Samples were cleaved *in situ* at 40 K in UHV. The data were acquired using a tunable VUV laser ARPES [29]. Momentum and energy resolution were set at ~0.005 $Å^{-1}$ and 2 meV. For first-principles band structure calculations, we used the Perdew-Burke-Ernzerhof parametrization of the generalized gradient approximation [34] and the full-potential (linearized) augmented plane-wave plus local orbitals [FP-(L)APW + LO] method including the spin-orbit coupling as implemented in the WIEN2K code [35]. Experimental crystal structure taken from Ref. [36] was used. The muffin-tin radii for W and Te atoms, r_W and r_{Te}, were set to 2.4 and 2.38 a.u., respectively. The maximum modulus for the reciprocal lattice vectors K_{max} was chosen so that $r_{Te}K_{max} = 9.00$. TEP was calculated using a $52 \times 29 \times 13$ k-point mesh with the BOLTZTRAP code [37].

Thermoelectric power.—The field dependence of the TEP at 2.2 K in WTe_2 shows very clear quantum oscillations [Fig. 1(a)], as was the case for $PtSn_4$ [13]. FFT analysis [Fig. 1(a) inset] gives $F^1 = 0.93$ MOe,

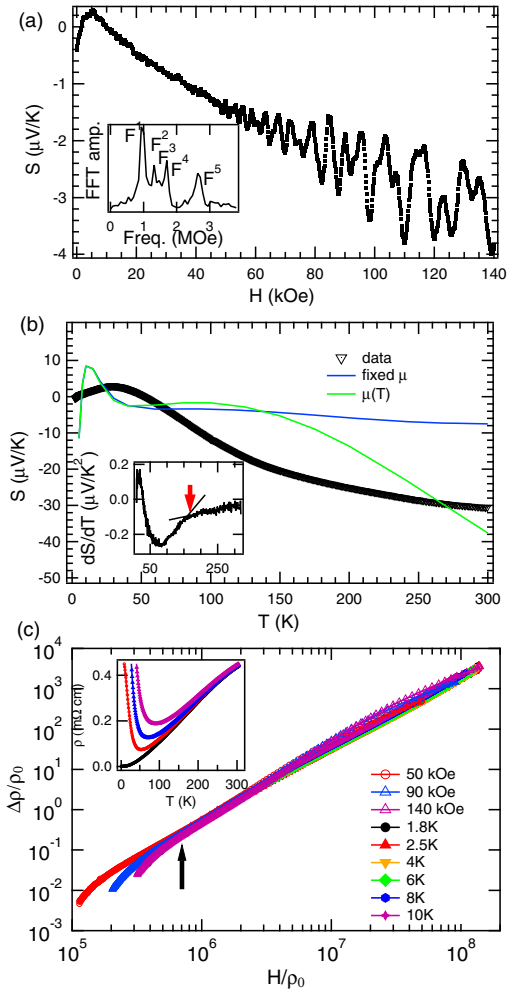

FIG. 1 (color online). (a) Magnetic field dependence of thermoelectric power (TEP) measured at $T = 2.2$ K showing very clear quantum oscillations. Inset shows FFT of data after subtraction of a smooth background. (b) Temperature dependence of TEP. Inset shows first derivative with arrow marking the change of slope due to Lifshitz transition. Calculated x component of TEP (i) with fixed chemical potential $\mu(T = 0)$ (blue line) and (ii) with temperature-dependent $\mu(T)$ (green line). In case (ii), $\mu(T)$ calculated from the actual electronic structure is scaled by a factor of 3 for the best experimental fit and shows a variation of 45 meV for temperatures between 0 and 300 K. (c) Generalized Kohler plot. Arrow marks the point below which the Kohler rule is violated ($T < 60$ K). Inset shows temperature dependence of the resistance measured for magnetic field of 0, 50, 90, and 140 kOe.

$F^2 = 1.31$ MOe, $F^3 = 1.47$ MOe, and $F^4 = 1.70$ MOe, in excellent agreement with the values found from Shubnikov–de Hass data (Fig. S2 in Supplemental Material [33]). Peaks F^1 and F^4 are attributed to hole pockets, while peaks F^2 and F^3 are due to nearly degenerate electron pockets [25]. The peak labeled F^5 is thought to be a result of the magnetic breakdown of F^1 and F^4 low field orbits [25].

The temperature dependence of the TEP in Fig. 1(b) shows two features that are noteworthy: (a) a nonmonotonic dependence of the TEP on temperature with a local maximum at ~30 K and (b) a kink at $T \sim 160$ K marked by an arrow in the inset of Fig. 1(b) observed in the rate of change of the TEP dS/dT as a function of temperature. This fact will be important when we investigate the electronic structure using ARPES. The solid green and blue lines are calculated TEP and are discussed later. We also note that the here-reported feature in TEP occurs at very similar temperature to one where the large magnetoresistance is suppressed [16].

Magnetoresistance.—The temperature and field dependence of the extraordinarily large MR of WTe_2 are shown in Fig. 1(c). The generalized Kohler's plot shows that there is fairly good scaling of the data with an exponent of ~1.98 at lower temperatures. As the temperature is increased, Kohler's scaling breaks down, as was also previously suggested [17], at the field indicated by the vertical arrow in Fig. 1(c); at this point temperatures range from 70 to 140 K for scans at different fields. We now proceed to elucidate the electronic origin of the change of the slope of the TEP and violation of Kohler's rule.

In the data discussed below, we provide evidence for two pairs of hole pockets and two pairs of electron pockets in ARPES. We then show the effect of increasing temperature, and how that enhances the electron pockets and finally the disappearance of the hole pockets, i.e., the Lifshitz transition observed at 160 K.

ARPES Fermi surface and band dispersion.—In Fig. 2(a) we show the ARPES intensity along high-symmetry directions in the Brillouin zone, integrated within 10 meV about the chemical potential, with the high intensity contours marking the location of the Fermi surface sheets. By comparing with our electronic structure calculations in Fig. 3(a), we observe that the ARPES data clearly resolve the two pairs of hole pockets; however, the separation between concentric electron pockets is too small and they appear as a single contour. The top of the band at Γ is located below the chemical potential for all studied photon energies and temperatures down to 20 K, as shown in Fig. S6 of the Supplemental Material [33].

In the band dispersion in Fig. 2(b), only the right branch of the electron band is clearly visible due to matrix elements. This is followed by two crossings of the left sides of the hole bands (marked by dashed lines), and then coinciding crossings of the right branch of both of the hole

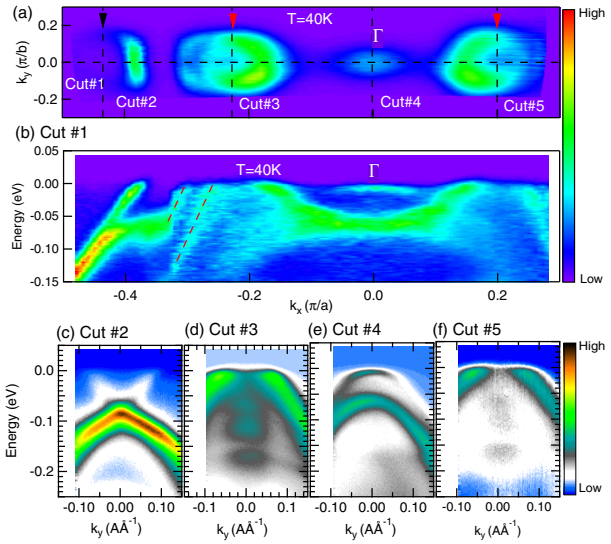

FIG. 2 (color online). Fermi surface plot and band dispersion measured at $T = 40$ K and photon energy of 5.77 eV. (a) Fermi surface plot of ARPES intensity integrated within 10 meV about the chemical potential. Black and red arrows point to electron and hole pockets, respectively. (b)–(f) Band dispersion along cuts 1–5. Dashed lines in (b) mark the two left branches of the two hole bands.

bands. At the center of the BZ, the top of the hole band is located just below the chemical potential; thus, there is no hole pocket at the center of the zone. Detailed band dispersions along vertical cuts are shown in Figs. 2(c)–2(f). Figure 2(c) shows that the bottom of the electron band joins with the top of a lower band and appears just like the structure of a Dirac state [38] approximately 70 meV below the chemical potential. This is different from calculations shown in Fig. 3(a), where the bottom of the electron pocket is separated from the band below by a 200 meV gap. Cut 3 and cut 5 reveal that the dispersions of the hole pockets are nearly degenerate at this location.

T-dependent ARPES and evidence for Lifshitz transition.—We now proceed to describe one of the more intriguing electronic properties of this material, a restructuring of the Fermi surface with increasing temperature, that also has consequences for the unusual transport properties.

Figure 3(a) shows the calculated band structure along the Γ-X direction. The band calculation predicts a pair of hole pockets and a doubly degenerate electron pocket between Γ and X, in agreement with ARPES data presented above and with previous calculations [16]. In Figs. 3(b) and 3(c) we show the Fermi surface map measured at 40 and 160 K. The hole pockets (marked by red arrows) shrink from two circles to a spot of intensity and electron pockets (marked by black arrow) expand with increasing temperature. We detail this behavior by plotting the ARPES intensity divided by the Fermi function along the vertical cut at the center of the hole pocket in Figs. 3(d)–3(k). A clearly

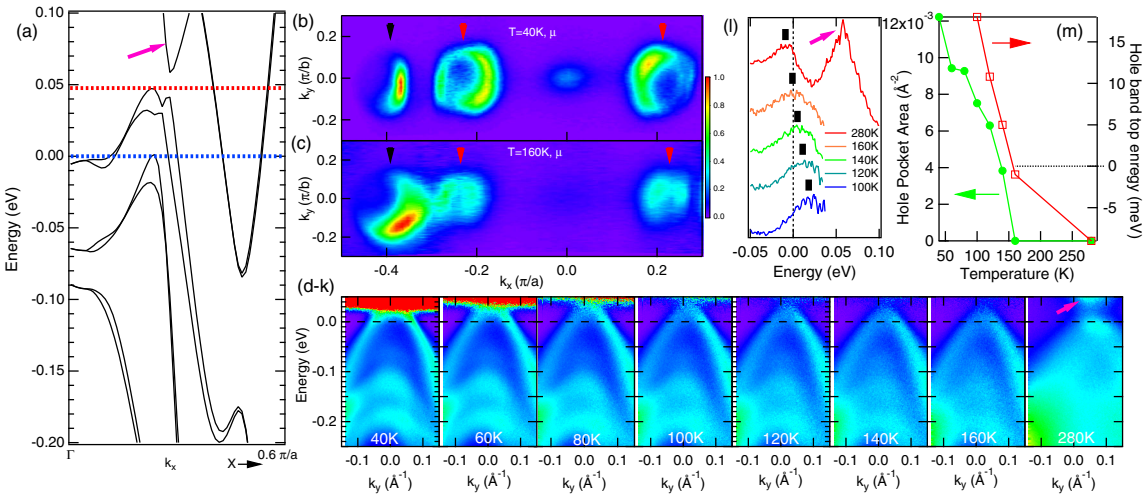

FIG. 3 (color online). (a) Calculated band structure along Γ-X symmetry direction. Blue and red dashed lines mark the values of chemical potential determined from ARPES data at low and high temperature, respectively. (b) Fermi surface plot of ARPES intensity integrated within 10 meV about the chemical potential measured at $T = 40$ K and 5.77 eV. Black and red arrows point to electron and hole pockets, respectively. (c) Same as (b) but for $T = 160$ K. (d)–(k) Temperature dependence of the band dispersion at the hole pocket [along cut 1 in Fig. 1(a)] divided by the Fermi function. (l) EDCs divided by Fermi function at the center of the hole pocket for several temperatures. Black line marks the energy of the peak. (m) Temperature dependence of the area of the hole pocket and energy of the top of the hole band. Purple arrows in (a), (l), and (k) point to a band located above the hole band.

visible hole band moves down in energy and by 160 K its top touches the chemical potential, and at a temperature of 280 K the top of this band has sunk below the chemical potential.

To quantify this effect we have plotted the Energy Distribution Curves (EDC) divided by the Fermi function at the center of the hole pocket for several temperatures in Fig. 3(l) and extracted the energy at the top of the hole band from a Gaussian fit in Fig. 3(m). Our data show that the top of the hole band moves down in energy upon increasing temperature from 18 meV at 120 K to −7 meV at 280 K. We have also extracted the area of the hole pocket by measuring the separation between Momentum Distribution Curves (MDC) peaks as a function of temperature in Fig. 3(m). We see that the top of the hole band moves below the chemical potential and the area of the hole pocket vanishes above ∼160 K, signaling the Lifshitz transition.

These data provide an archetypical example of a temperature-induced Lifshitz transition since they demonstrate a change of the Fermi surface topology upon heating. Chemical-substitution-induced Lifshitz transitions are quite common and were previously observed in $Ba(Fe_{1-x}Co_x)_2As_2$ at Co concentrations of 3.8%, 11%, and 20% [3,4]. On the other hand, a temperature-induced Lifshitz transition in the absence of a structure or magnetic phase transition is extremely rare. The temperature-dependent TEP, in particular the change of slope of $\partial S/\partial T$ at ∼160 K (Fig. 1, inset), is consistent with the existence of a temperature-induced Lifshitz transition, as TEP is expected to be very sensitive to the changes in the Fermi surface topology [39].

T dependence of chemical potential $\mu(T)$.—The dramatic temperature-dependent change in relative size of the electron and hole pockets manifests itself in other measurements over wider temperature ranges, as we discuss below. Going back to Fig. 1(b), we compare the TEP measurements with our calculations of the x component of TEP. We notice that for a fixed $\mu(T) = 0$, the agreement is rather poor: the TEP has a large positive peak at low temperatures, and is almost temperature independent above ∼50 K [blue curve in Fig. 1(b)], quite unlike the behavior seen in the experimental TEP data.

We next calculate the temperature-dependent $\mu(T)$, by imposing a fixed total number of electrons across all bands at all temperatures. In conventional metals, μ does not change appreciably for $k_BT \ll E_F$. However, in WTe_2 and other semimetals, where the top of the hole band and bottom of the electron band are in close proximity (few tens of meV) to the chemical potential, significant changes of $\mu(T)$ with temperature can occur; e.g., in WTe_2 we calculate that chemical potential should shift by 14 meV between $T = 0$ K and $T = 300$ K. We have repeated the calculation of TEP using a scaled $\mu_F(T = 300\text{K}) = 45$ meV to account for possible renormalization effects and match the experimentally observed shifts. We then use such obtained $\mu_F(T)$ to calculate the x component of TEP. When the temperature-induced shifts of the chemical potential are taken into account, the absolute value of TEP increases monotonically at high temperatures with qualitatively improved agreement with the measurements [green line in Fig. 1(b)]. Although the calculation does not take into account the thermal expansion, phonon drag [40], and assumes constant relation time (i.e., ignores

T-dependent scattering), it does reproduce the key features of the TEP data: the positive peak at low temperatures and the correct trend at higher temperatures. The breakdown of Kohler's rule in MR shown in Fig. 1(c) can also be understood in terms of the changing ratio of electron and hole carriers implied by the data in Fig. 3(m) and caused by the temperature-induced shift of $\mu(T)$.

In summary, we discovered the temperature-driven Lifshitz transition in highly magnetoresistive WTe_2. By correlating spectroscopic studies with electronic structure calculations, we find that the chemical potential can be strongly temperature dependent in semimetallic materials such as WTe_2, which in turn can strongly affect their magnetotransport properties [16] by driving a Lifshitz transition. Such shifts in μ with temperature were previously reported in pnictides' high-temperature superconductors [41,42], where both electron and hole pockets were found in close proximity to the chemical potential. The mechanisms described here, the presence of small electron and hole pockets, strong chemical potential shifts, and Lifshitz transitions, are likely to be relevant for other systems, such as 3D Dirac semimetals, Weyl semimetals, and thermoelectric materials. In the presence of interactions, the restructured Fermi surfaces could change the nesting conditions and drive various magnetic, charge-ordered, and superconducting transitions in these classes of dichalcogenide and related materials.

We would like to thank Mohit Randeria for very useful discussions. Research was supported by the U.S. Department of Energy, Office of Basic Energy Sciences, Division of Materials Sciences and Engineering. Ames Laboratory is operated for the U.S. Department of Energy by the Iowa State University under Contract No. DE-AC02-07CH11358. N. H. J. is supported by the Gordon and Betty Moore Foundation EPiQS Initiative (Grant No. GBMF4411). Work at Ohio State University and L. H. were supported by CEM, a NSF MRSEC, under Grant No. DMR-1420451.

*canfield@ameslab.gov
†kaminski@ameslab.gov

[1] Y. Okada, M. Serbyn, H. Lin, D. Walkup, W. Zhou, C. Dhital, M. Neupane, S. Xu, Y. J. Wang, R. Sankar, F. Chou, A. Bansil, M. Z. Hasan, S. D. Wilson, L. Fu, and V. Madhavan, Science **341**, 1496 (2013).
[2] I. Zeljkovic, Y. Okada, C.-Y. Huang, R. Sankar, D. Walkup, W. Zhou, M. Serbyn, F. Chou, W.-F. Tsai, H. Lin, A. Bansil, L. Fu, M. Z. Hasan, and V. Madhavan, Nat. Phys. **10**, 572 (2014).
[3] C. Liu, T. Kondo, R. M. Fernandes, A. D. Palczewski, E. D. Mun, N. Ni, A. N. Thaler, A. Bostwick, E. Rotenberg, J. Schmalian, S. L. Bud'ko, P. C. Canfield, and A. Kaminski, Nat. Phys. **6**, 419 (2010).
[4] C. Liu, A. D. Palczewski, R. S. Dhaka, T. Kondo, R. M. Fernandes, E. D. Mun, H. Hodovanets, A. N. Thaler, J. Schmalian, S. L. Bud'ko, P. C. Canfield, and A. Kaminski, Phys. Rev. B **84**, 020509 (2011).
[5] S. L. Bud'ko, A. N. Voronovskii, A. G. Gapotchenko, and E. S. Itskevich, Zh. Eksp. Teor. Fiz. **86**, 778 (1984). [Sov. Phys. JETP **59**, 454 (1984)].
[6] D. Kang, Y. Zhou, W. Yi, C. Yang, J. Guo, Y. Shi, S. Zhang, Z. Wang, C. Zhang, S. Jiang, A. Li, K. Yang, Q. Wu, G. Zhang, L. Sun, and Z. Zhao, Nat. Commun. **6**, 7804 (2015).
[7] M. N. Baibich, J. M. Broto, A. Fert, F. Nguyen Van Dau, F. Petroff, P. Etienne, G. Creuzet, A. Friederich, and J. Chazelas, Phys. Rev. Lett. **61**, 2472 (1988).
[8] G. Binasch, P. Grünberg, F. Saurenbach, and W. Zinn, Phys. Rev. B **39**, 4828 (1989).
[9] A. Urushibara, Y. Moritomo, T. Arima, A. Asamitsu, G. Kido, and Y. Tokura, Phys. Rev. B **51**, 14103 (1995).
[10] Y. Moritomo, A. Asamitsu, H. Kuwahara, and Y. Tokura, Nature (London) **380**, 141 (1996).
[11] A. P. Ramirez, R. J. Cava, and J. Krajewski, Nature (London) **386**, 156 (1997).
[12] J. Daughton, J. Magn. Magn. Mater. **192**, 334 (1999).
[13] E. Mun, H. Ko, G. J. Miller, G. D. Samolyuk, S. L. Bud'ko, and P. C. Canfield, Phys. Rev. B **85**, 035135 (2012).
[14] T. Liang, Q. Gibson, M. N. Ali, M. Liu, R. J. Cava, and N. P. Ong, Nat. Mater. **14**, 280 (2015).
[15] K. Wang, D. Graf, L. Li, L. Wang, and C. Petrovic, Sci. Rep. **4**, 7328 (2014).
[16] M. N. Ali, J. Xiong, S. Flynn, J. Tao, Q. D. Gibson, L. M. Schoop, T. Liang, N. Haldolaarachchige, M. Hirschberger, N. P. Ong, and R. J. Cava, Nature (London) **514**, 205 (2014).
[17] Y. Zhao, H. Liu, J. Yan, W. An, J. Liu, X. Zhang, H. Wang, Y. Liu, H. Jiang, Q. Li, Y. Wang, X.-Z. Li, D. Mandrus, X. C. Xie, M. Pan, and J. Wang, Phys. Rev. B **92**, 041104 (2015).
[18] L. R. Thoutam, Y. L. Wang, Z. L. Xiao, S. Das, A. Luican-Mayer, R. Divan, G. W. Crabtree, and W. K. Kwok, Phys. Rev. Lett. **115**, 046602 (2015).
[19] X.-C. Pan, Y. Pan, J. Jiang, H. Zuo, H. Liu, X. Chen, Z. Wei, S. Zhang, Z. Wang, X. Wan, Z. Yang, D. Feng, Z. Xia, L. Li, F. Song, B. Wang, Y. Zhang, and G. Wang, arXiv:1505.07968v1.
[20] I. Pletikosic, M. N. Ali, A. V. Fedorov, R. J. Cava, and T. Valla, Phys. Rev. Lett. **113**, 216601 (2014).
[21] P. S. Alekseev, A. P. Dmitriev, I. V. Gornyi, V. Y. Kachorovskii, B. N. Narozhny, M. Schütt, and M. Titov, Phys. Rev. Lett. **114**, 156601 (2015).
[22] S. Kabashima, J. Phys. Soc. Jpn. **21**, 945 (1966).
[23] L. Brixner, J. Inorg. Nucl. Chem. **24**, 257 (1962).
[24] J. Augustin, V. Eyert, T. Böker, W. Frentrup, H. Dwelk, C. Janowitz, and R. Manzke, Phys. Rev. B **62**, 10812 (2000).
[25] Z. Zhu, X. Lin, J. Liu, B. Fauqué, Q. Tao, C. Yang, Y. Shi, and K. Behnia, Phys. Rev. Lett. **114**, 176601 (2015).
[26] F.-X. Xiang, M. Veldhorst, S.-X. Dou, and X.-L. Wang, arXiv:1504.01460v1.
[27] P. L. Cai, J. Hu, L. P. He, J. Pan, X. C. Hong, Z. Zhang, J. Zhang, J. Wei, Z. Q. Mao, and S. Y. Li, Phys. Rev. Lett. **115**, 057202 (2015).
[28] J. Jiang, F. Tang, X. C. Pan, H. M. Liu, X. H. Niu, Y. X. Wang, D. F. Xu, H. F. Yang, B. P. Xie, F. Q. Song, X. G. Wan, and D. L. Feng, preceding Letter, Phys. Rev. Lett. **115**, 166601 (2015).

[29] R. Jiang, D. Mou, Y. Wu, L. Huang, C. D. McMillen, J. Kolis, H. G. Giesber, J. J. Egan, and A. Kaminski, Rev. Sci. Instrum. **85**, 033902 (2014).
[30] B. E. Brown, Acta Crystallogr. **20**, 268 (1966).
[31] P. C. Canfield and Z. Fisk, Philos. Mag. B **65**, 1117 (1992).
[32] E. Mun, S. L. Bud'ko, M. S. Torikachvili, and P. C. Canfield, Meas. Sci. Technol. **21**, 055104 (2010).
[33] See Supplemental Material at http://link.aps.org/supplemental/10.1103/PhysRevLett.115.166602 for technical details of the experiment and calculations, additional transport data and photon energy dependent ARPES data.
[34] J. P. Perdew, K. Burke, and M. Ernzerhof, Phys. Rev. Lett. **77**, 3865 (1996).
[35] P. Blaha, K. Schwarz, G. Madsen, D. Kvasnicka, and J. Luitz, *WIEN2K, An Augmented Plane Wave+Local Orbitals Program for Calculating Crystal Properties*, edited by K. Schwarz (Technische Universität Wien, Austria, 2001).
[36] A. Mar, S. Jobic, and J. A. Ibers, J. Am. Chem. Soc. **114**, 8963 (1992).
[37] G. K. H. Madsen and D. J. Singh, Comput. Phys. Commun. **175**, 67 (2006).
[38] A. K. Geim and K. S. Novoselov, Nat. Mater. **6**, 183 (2007).
[39] A. Varlamov, V. Egorov, and A. Pantsulaya, Adv. Phys. **38**, 469 (1989).
[40] R. D. Barnard, *Thermoelectricity in Metals and Alloys* (Taylor and Francis, London, 1972).
[41] R. S. Dhaka, S. E. Hahn, E. Razzoli, R. Jiang, M. Shi, B. N. Harmon, A. Thaler, S. L. Bud'ko, P. C. Canfield, and A. Kaminski, Phys. Rev. Lett. **110**, 067002 (2013).
[42] V. Brouet, P.-H. Lin, Y. Texier, J. Bobroff, A. Taleb-Ibrahimi, P. LeFevre, F. Bertran, M. Casula, P. Werner, S. Biermann, F. Rullier-Albenque, A. Forget, and D. Colson, Phys. Rev. Lett. **110**, 167002 (2013).